Shitomi, T.; Garro, E.; Murayama, K.; Gomez-Barquero, D. (2018). MIMO Scattered Pilot Performance and Optimization for ATSC 3.0. IEEE Transactions on Broadcasting. 64(2):188-200. https://doi.org/10.1109/TBC.2017.2755262

MIMO Scattered Pilot Performance and Optimization for ATSC 3.0

Takuya Shitomi, Eduardo Garro, Kenichi Murayama and David Gomez-Barquero

***Abstract*— ATSC 3.0 is the latest Digital Terrestrial Television (DTT) standard, and it allows a higher spectral efficiency and/or a transmission robustness with Multiple-Input Multiple-Output (MIMO) technology compared to existing DTT standards. Regarding MIMO channel estimation, two pilot encoding algorithms known as Walsh-Hadamard encoding and Null Pilot encoding are possible in ATSC 3.0. The two MIMO pilot algorithms are standardized so as to have the same pilot positions and the same pilot boosting as SISO, and the optimum pilot configuration has not been fully evaluated for MIMO. This paper focuses on the performance evaluation and optimization of the pilot boosting and the pilot patterns for two MIMO pilot encoding algorithms in ATSC 3.0 using physical layer simulations. This paper provides a great benefit to broadcasters to select the MIMO pilot configuration including pilot boosting, pilot pattern and pilot encoding algorithm that better suits their service requirements. Several channel interpolation algorithms have been taken into account as a typical receiver implementation in both fixed SFN reception and mobile reception.**

***Index Terms*—ATSC3.0, terrestrial broadcasting, MIMO, channel estimation, pilot pattern.**

I. Introduction

ATSC 3.0, the next-generation Digital Terrestrial Television (DTT) standard, allows a higher spectral efficiency and/or a transmission robustness with Multiple-Input Multiple-Output (MIMO) technology [1]. MIMO technology was first time ever introduced in DTT specification DVB-NGH [2] and it has been further developed and fully standardized in ATSC 3.0 [3]. MIMO technology provides a higher spectral efficiency via spatial multiplexing, and/or higher transmission robustness via spatial diversity. This higher flexibility allows broadcasters to select the configuration that better suits the capacity and coverage requirements per service. In practice, MIMO in DTT is implemented using cross-polarized 2x2 MIMO, i.e. horizontal and vertical polarization to decorrelate the channel even in Line-of-Sight (LOS) reception conditions [4].

2x2 MIMO spatial multiplexing requires doubling the pilot overhead compared to Single-Input Single-Output (SISO) to keep the channel estimation performance. DVB-NGH adopted an orthogonal scattered pilot encoding scheme, namely Walsh-Hadamard (WH) encoding, which is the same configuration used in DVB-T2 for Multiple-Input Single-Output (MISO) mode [5]. ATSC 3.0 adopted WH encoding for MIMO channel estimation together with another scattered pilot encoding algorithm known as Null Pilot (NP) encoding [3]. The NP encoding scheme was firstly standardized in 4G Long Term Evolution (LTE) [6] for MIMO mode. However, the scheme was modified and first time ever introduced in DTT specification ATSC 3.0. The MIMO pilot positions in 4G LTE are different from SISO depending on the antenna configuration. On the other hand, the MIMO pilot positions in ATSC 3.0 are located at the same positions as SISO and the pilot positions are selectable out of 16 pilot patterns. Another novelty of pilot configuration in ATSC 3.0 is that the pilot boosting is selectable out of five pilot boosting values.

The selection of the optimum MIMO pilot configuration (pilot encoding scheme, pilot pattern and pilot boosting) is not straightforward, and it represents a trade-off between quality of the channel estimation and overhead. The pilots must be sufficiently dense to follow channel fluctuations, but the denser pilots reduce the net transmission capacity. Although different studies have shown the pilot optimization for SISO in ATSC 3.0, see e.g. [7], the impact of pilot encoding for MIMO transmission has not been fully evaluated. Indeed, the two pilot encoding algorithms were not deeply compared in the standardization process in terms of the channel estimation algorithms and channel conditions [3]. Moreover, the MIMO pilots are directly standardized so as to have the same positions (pilot patterns) and the same amplitudes (pilot boosting) as SISO.

Regarding the MIMO pilot configuration, five different boosting values are available per 16 different pilot patterns for each pilot encoding algorithm. This paper focuses on the performance and optimization on the pilot boosting, pilot pattern and the MIMO pilot encoding algorithms considering the channel interpolation method at the receiver. It should be noted that the analysis on the optimum pilot boosting for both MIMO pilot encoding algorithms for ATSC 3.0 is novel because the performance has not been evaluated in literature until now. The study greatly contributes to the selecting the

Manuscript received May 26, 2017; revised Aug. 15, 2017. Accepted Aug. 29, 2017. Parts of this paper have been published in the Proceedings of the IEEE International Symposium on Broadband Multimedia Systems and Broadcasting, Cagliari, Italy, in 2017.

This work was partially supported by the Ministry of Economy and Competitiveness of Spain (TEC2014-56483-R), co-funded by the European FEDER fund.

T. Shitomi and K. Murayama are with Japan Broadcasting Corporation (NHK), Tokyo, Japan (email: shitomi.t-gy@nhk.or.jp; murayama.k-fu@nhk.or.jp).

T. Shitomi, E. Garro and D. Gomez-Barquero are with the Universitat Politecnica de Valencia, 46022 Valencia, Spain (e-mail: tashi1@iteam.upv.es; edgarcre@iteam.upv.es; dagobar@iteam.upv.es).

pilot configuration in ATSC3.0, because the newly introduced NP encoding algorithm has not been evaluated and compared with Walsh-Hadamard so far. The performance is evaluated with the plain spatial multiplexing standardized in ATSC 3.0. The main contribution of this paper is to provide a guideline on MIMO pilot configuration in ATSC3.0 for broadcasters.

The optimum pilot boosting is theoretically deduced and evaluated by physical layer simulations with an ATSC 3.0 simulator. The evaluations of the pilot pattern and the encoding algorithm are extracted from physical layer simulations in both fixed and mobile reception scenarios.

The paper is structured as follows: Section II reviews the ATSC 3.0 waveform parameters to be considered in this paper. The channel estimation method for ATSC3.0 MIMO transmission is presented in Section III. Section IV presents the theoretical analysis on MIMO pilot boosting. Section V describes the methodology and the simulation setup. The simulation results evaluated by simulation are presented in Section VI. The conclusions are summarized in Section VII.

II. ATSC 3.0 Waveform Overview

Fig. 1 presents the block diagram of 2x2 MIMO transmitter in ATSC 3.0. The input bit stream passes through a Bit-Interleaved Coded Modulation (BICM) chain. The BCIM provides two symbol streams to be transmitted on antenna #1 and #2. In the Framing & Interleaving chain, the input symbol streams are time-interleaved and frequency-interleaved. The Framing & Interleaving chains of both antennas have the same configuration. The Waveform Generation chain is composed of pilots insertion, Inverse Fast Fourier Transform (IFFT) and Guard Interval (GI) insertion blocks. Fig. 2 shows the block diagram of the receiver. The active symbol period is extracted from the received signals, which are then converted into frequency domain signals by the Fast Fourier Transform (FFT). The channel estimation is conducted using the MIMO pilots. The received signals are equalized and demultiplexed by MIMO detection. The details of the Waveform Generation parameters are described below.

A. Pilots

Table I gives an overview of the different types of pilots and the corresponding MIMO pilot encoding mechanism per antenna. Pilots for MIMO fall on exactly the same positions as for SISO, but the amplitudes and/or phases of the scattered, continual, edge, and subframe boundary pilots may be modified compared to SISO. The scattered pilots are used for channel estimation, and they are regularly inserted in time and frequency direction. The common and additional continual pilots are transmitted on predefined carriers, and they are basically used for synchronization at the receiver. The edge pilots are transmitted on the both edge carriers to complete the frequency interpolation procedure in the channel estimation. The subframe boundary pilots are transmitted on the last OFDM symbol of a subframe to terminate the time interpolation procedure in the channel estimation. The WH algorithm differs from NP only in the scattered and the additional continual pilots. In Table I, SISO indicates that the pilots are not modified compared to the pilots used in SISO configuration. The details of pilot encoding algorithms WH and NP are described in Section III.

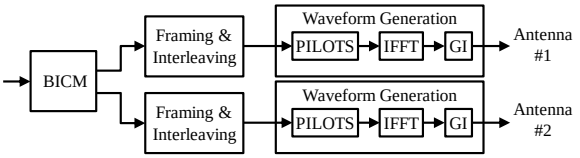

Fig. 1. Block diagram of ATSC 3.0 MIMO transmitter.

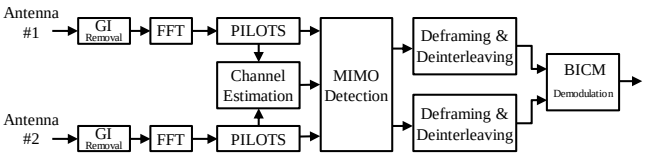

Fig. 2. Block diagram of ATSC 3.0 MIMO receiver.

TABLE I
MIMO Pilots Overview

Pilot Encoding Algorithm	Antenna	Scattered Pilot	Common Continual Pilot	Additional Continual Pilot	Edge Pilot	Subframe Boundary Pilot
WH	#1	SISO	SISO	SISO	SISO	SISO
	#2	WH	SISO	SISO/WH	WH	WH
NP	#1	NP	SISO	SISO	SISO	SISO
	#2	NP	SISO	SISO/NP	WH	WH

TABLE II
Allowed SP Patterns for Walsh-Hadamard Encoding

GI Pattern	GI Samples	8K FFT	16K FFT	32K FFT
GI1_192	192	MP16_2, MP16_4, MP8_2, MP8_4	MP16_2, MP16_4	MP16_2
GI2_384	384	MP8_2, MP8_4, MP4_2, MP4_4	MP16_2, MP16_4, MP8_2, MP8_4	MP16_2
GI3_512	512	MP6_2, MP6_4, MP3_2, MP3_4	MP12_2, M12_4, MP6_2, MP6_4	MP12_2
GI4_768	768	MP4_2, MP4_4	M8_2, M8_4, MP4_2, MP4_4	MP16_2, MP8_2
GI5_1024	1024	MP3_2, MP3_4	MP6_2, MP6_4, MP3_2, MP3_4	MP12_2, MP6_2
GI6_1536	1536	N/A	MP4_2, MP4_4	MP8_2, MP4_2
GI7_2048	2048	N/A	MP3_2, MP3_4	MP6_2, MP3_2
GI8_2432	2432	N/A	MP3_2, MP3_4	MP6_2, MP3_2
GI9_3072	3072	N/A	N/A	MP3_2
GI10_3648	3648	N/A	N/A	MP3_2
GI11_4096	4096	N/A	N/A	MP3_2
GI12_4864	4864	N/A	N/A	MP3_2

The terminology employed for the MIMO pilot patterns is described as MPa_b, where a = D_X and b = D_Y are defined. D_X is the number of carriers between the scattered pilot bearing carriers and D_Y is the number of symbols between the scattered pilots in a single pilot bearing carrier. Taking the Nyquist limits

TABLE III
ALLOWED SP PATTERNS FOR NULL PILOT ENCODING

GI Pattern	GI Samples	8K FFT	16K FFT	32K FFT
GI1_192	192	MP32_2, MP32_4, MP16_2, MP16_4	MP32_2, MP32_4	MP32_2
GI2_384	384	MP16_2, MP16_4, MP8_2, MP8_4	MP32_2, MP32_4, MP16_2, MP16_4	MP32_2
GI3_512	512	MP12_2, MP12_4, MP6_2, MP6_4	MP24_2, MP24_4, MP12_2, MP12_4	MP24_2
GI4_768	768	MP8_2, MP8_4, MP4_2, MP4_4	MP16_2, MP16_4, MP8_2, MP8_4	MP32_2, MP16_2
GI5_1024	1024	MP6_2, MP6_4, MP3_2, MP3_4	MP12_2, MP12_4, MP6_2, MP6_4	MP24_2, MP12_2
GI6_1536	1536	MP4_2, MP4_4	MP8_2, MP8_4, MP4_2, MP4_4	MP16_2, MP8_2
GI7_2048	2048	MP3_2, MP3_4	MP6_2, MP6_4, MP3_2, MP3_4	MP12_2, MP6_2
GI8_2432	2432	N/A	MP6_2, MP6_4, MP3_2, MP3_4	MP12_2, MP6_2
GI9_3072	3072	N/A	MP4_2, MP4_4	MP8_2, MP3_2
GI10_3648	3648	N/A	MP4_2, MP4_4	MP8_2, MP3_2
GI11_4096	4096	N/A	MP3_2, MP3_4	MP6_2, MP3_2
GI12_4864	4864	N/A	N/A	MP6_2, MP3_2

into account, the SP patterns allowed for the GI/FFT combinations with WH encoding for MIMO are presented in Table II. Compared with the table for SISO [7], D_X is reduced to half to keep the Nyquist limits for WH. The SP patterns for NP encoding is shown in Table III. The combination of D_X and D_Y are the same as in SISO.

B. *Inverse Fast Fourier Transform*

ATSC 3.0 has adopted three different FFT sizes: 8k, 16k and 32k. OFDM systems are sensitive to inter-carrier interference (ICI), and the sensitivity depends on the FFT size. The smaller the FFT size, the more ICI the system can withstand. On the other hand, the smaller FFT size has a drawback to introduce the higher overhead of GI compared with the higher FFT size.

C. *Guard Interval*

ATSC 3.0 has adopted twelve GI lengths: 192, 384, 512, 768, 1024, 1536, 2048, 2432, 3072, 3648, 4096, and 4864 samples. GI length must be, at least, equal to the length of the delay time between the multipath signals in order to eliminate inter-symbol interference (ISI), which is also important for Single Frequency Network (SFN). The further separation between the transmitters is allowed with the longer GI duration, i.e. the larger SFN area can be realized. However, the longer GI also increases the overhead. Thus, not all GI lengths are allowed for the three FFT sizes.

III. CHANNEL ESTIMATION IN ATSC 3.0

As the result of pilot encoding process, MIMO pilots are divided into two subsets (one per antenna). The two subsets are designed to be orthogonal in phase or amplitude to observe the channel separately. The details of the channel estimation parameters are described as follows.

A. *Pilot Encoding*

Fig. 3 illustrates the MIMO scattered pilot MP3_2, i.e. D_X = 3, D_Y = 2, for WH encoding and NP encoding. The differences between the two MIMO pilot encoding algorithms are described next.

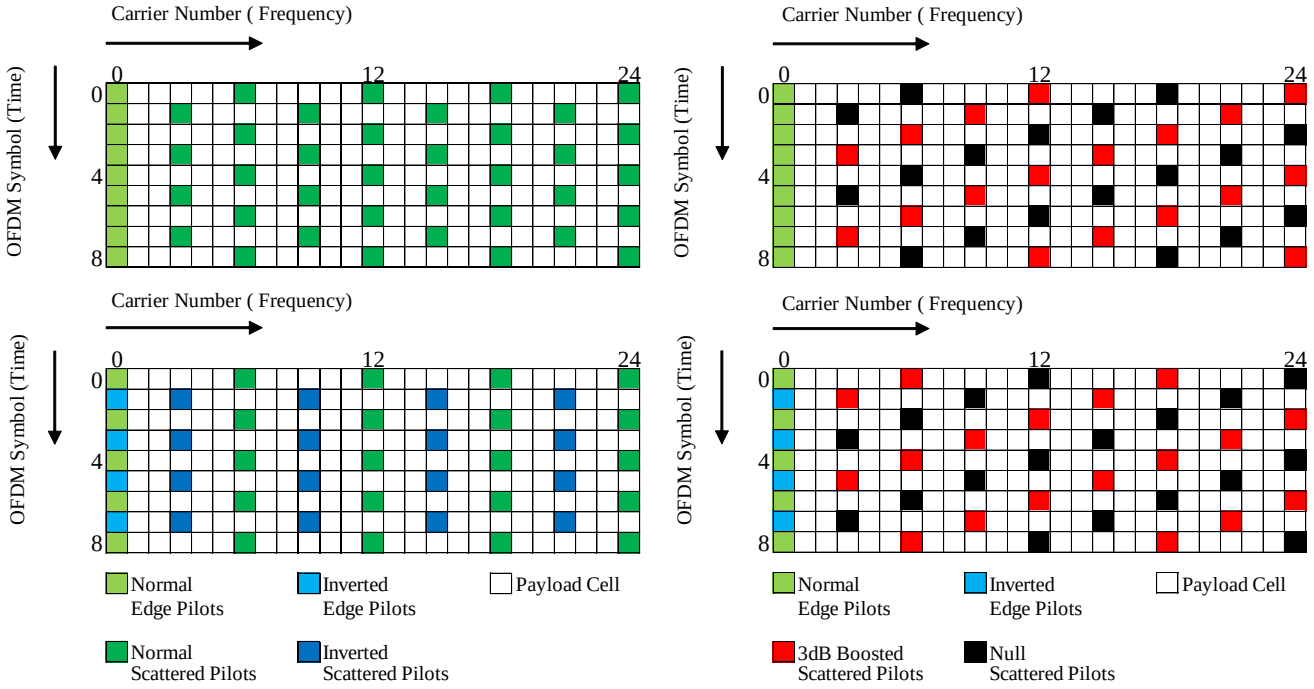

Fig. 3. MIMO pilots for Walsh-Hadamard encoding (left) and Null Pilot encoding (right). For Antenna #1 (top) and #2 (bottom).

1) Walsh-Hadamard

With WH encoding, the phases of all pilots transmitted from antenna #1 are not modified. Regarding the signal transmitted from antenna #2, the pilots can be partitioned into two subsets, and the phases of the scattered pilots are inverted every second pilot bearing carrier. That results that the half of scattered pilots transmitted from antenna #2 are not modified and that the other half pilots are inverted. As the result of the phase inversion on every second pilot bearing carrier, the number of carriers between the scattered pilot bearing carriers in each subset is doubled.

2) Null Pilot

With NP encoding, the amplitudes of the scattered pilots of both subsets are modified in both signals transmitted from antennas #1 and #2. With NP encoding, antenna #1 alternately transmits scattered pilots with 3 dB increased transmit power and scattered pilots with null power (zero amplitude). Scattered pilots of antenna #2 are transmitted with null power and with 3 dB gain in reverse order. The 3 dB boosting keeps the total signal power of the scattered pilot to be the same as SISO.

B. Channel Estimation

2x2 MIMO OFDM system can be modeled as

$$\mathbf{y} = \mathbf{H}\mathbf{x} + \mathbf{n}$$
$$\begin{bmatrix} y_1 \\ y_2 \end{bmatrix} = \begin{bmatrix} h_{11} & h_{12} \\ h_{21} & h_{22} \end{bmatrix} \begin{bmatrix} x_1 \\ x_2 \end{bmatrix} + \begin{bmatrix} n_1 \\ n_2 \end{bmatrix} \quad (1)$$

where **y** is the received symbol vector, **H** the Channel Frequency Response (CFR) matrix, **x** the transmitted symbol vector, and **n** the AWGN noise vector. y_i is the received symbol for receiving antenna #*i*, x_j the transmitted symbol for transmitting antenna #*j*, n_i the noise for receiving antenna #*i*. h_{ij} denotes the CFR from transmitting antenna #*j* to receiving antenna #*i*.

The first channel estimation step is to estimate the Channel Frequency Responses (CFRs) at the scattered pilot positions. A basic technique is the Least Square (LS) estimation, which does not exploit the correlation of the channel across frequency and time [8]. The next step is channel interpolation. In order to reduce the complexity, channel interpolation is performed with a cascade of two 1-dimentional operations. First operation is a linear time interpolation to obtain the CFRs at scattered pilot bearing carriers. Linear interpolation is a common option for time interpolation, since it only requires two points to be known. The second is frequency interpolation. Here, two common interpolations are investigated for the frequency interpolation. One option is linear interpolation which is the computationally least expensive, but provides poor interpolation in cases where the data to be interpolated is non-linear. The second option is Discrete Fourier Transform (DFT) interpolation [9], [10]. The frequency interpolation is applied to fulfill the CFRs for all data carriers in a single OFDM symbol.

Taking into account the interpolation operations mentioned above and the characteristics of both MIMO pilot encoding algorithms, the equivalent values of D_X and D_Y after channel interpolation are summarized in Table IV. The channel estimation with each pilot encoding algorithm is explained as follows.

TABLE IV
EQUIVALENT D_X AND D_Y IN MIMO PILOTS

SISO	MIMO	
	Walsh-Hadamard encoding	Null Pilot encoding
D_X	$2D_X$	D_X
D_Y	D_Y	$2D_Y$

1) Walsh-Hadamard

The resulting CFRs obtained by LS estimation are the sum or the difference of the two subsets, because the phase inversion is applied in WH encoding scheme. k_{sum}, the set of carrier index on which normal scattered pilots are transmitted from antenna #2 in Fig.3 (left, bottom), is defined as $k_{sum} = 2 \times N \times D_X$. where N is a non-negative integer (N=1, 2, …). The sum of the two CFRs is estimated from the scattered pilots on the carrier number k_{sum} of the OFDM symbol number l_{sum} as:

$$\tilde{h}_{sum1}[l_{sum}, k_{sum}] = \frac{y_1[l_{sum}, k_{sum}]}{x_1[l_{sum}, k_{sum}]} = h_{sum1}[l_{sum}, k_{sum}] + \frac{n_1[l_{sum}, k_{sum}]}{x_1[l_{sum}, k_{sum}]} \quad (2)$$
$$\tilde{h}_{sum2}[l_{sum}, k_{sum}] = \frac{y_2[l_{sum}, k_{sum}]}{x_1[l_{sum}, k_{sum}]} = h_{sum2}[l_{sum}, k_{sum}] + \frac{n_2[l_{sum}, k_{sum}]}{x_1[l_{sum}, k_{sum}]}$$

where $h_{sum1} = h_{11} + h_{12}$, $h_{sum2} = h_{21} + h_{22}$ [11]. l_{sum} is the OFDM symbol number which satisfies $k_{sum} \bmod (D_X \times D_Y) = D_X \times (l_{sum} \bmod D_Y)$. $\tilde{h}_{sum1}$ and $\tilde{h}_{sum2}$ are obtained for the scattered pilot cell as the LS estimations of h_{sum1} and h_{sum2}, respectively. On the other hand, the difference between the two channel responses is estimated from the scattered pilots on the carrier number $k_{dif} = (2 \times N - 1) \times D_X$ of the OFDM symbol number l_{dif} as:

$$\tilde{h}_{dif1}[l_{dif}, k_{dif}] = \frac{y_1[l_{dif}, k_{dif}]}{x_1[l_{dif}, k_{dif}]} = h_{dif1}[l_{dif}, k_{dif}] + \frac{n_1[l_{dif}, k_{dif}]}{x_1[l_{dif}, k_{dif}]} \quad (3)$$
$$\tilde{h}_{dif2}[l_{dif}, k_{dif}] = \frac{y_2[l_{dif}, k_{dif}]}{x_1[l_{dif}, k_{dif}]} = h_{dif2}[l_{dif}, k_{dif}] + \frac{n_2[l_{dif}, k_{dif}]}{x_1[l_{dif}, k_{dif}]}$$

where $h_{dif1} = h_{11} - h_{12}$, $h_{dif2} = h_{21} - h_{22}$. l_{dif} is the OFDM symbol number which satisfies $k_{dif} \bmod (D_X \times D_Y) = D_X \times (l_{dif} \bmod D_Y)$. $\tilde{h}_{dif1}$ and $\tilde{h}_{dif2}$ are obtained for the scattered pilot cell as the LS estimations of h_{dif1} and h_{dif2}, respectively. In order to obtain the estimates of the sum and difference of the CFR on all cells, time interpolation is performed first on every pilot bearing carrier. Next, frequency interpolation is performed separately on each subset, i.e. sum and difference estimates. After the 2-dimentional interpolation, the sum and difference estimates $\hat{h}_{sum1}$, $\hat{h}_{sum2}$, $\hat{h}_{dif1}$ and $\hat{h}_{dif2}$ are obtained for each cell, and the estimated CFR matrix, i.e. $\hat{h}_{11}$, $\hat{h}_{12}$, $\hat{h}_{21}$ and $\hat{h}_{22}$, can be obtained for each cell as below.

$$\begin{bmatrix} \hat{h}_{11} & \hat{h}_{12} \\ \hat{h}_{21} & \hat{h}_{22} \end{bmatrix} = \frac{1}{2} \begin{bmatrix} \hat{h}_{sum1} + \hat{h}_{dif1} & \hat{h}_{sum1} - \hat{h}_{dif1} \\ \hat{h}_{sum2} + \hat{h}_{dif2} & \hat{h}_{sum2} - \hat{h}_{dif2} \end{bmatrix} \quad (4)$$

Consequently, the Nyquist limit of the channel estimation in

frequency falls to half compared to the uncoded scattered pilot in SISO.

2) Null Pilot

The CFRs from transmitting antenna #1 to receiving antenna #1 and #2 (h_{11} and h_{21}) are estimated on the 3 dB boosted scattered pilots transmitted by antenna #1 as:

$$\tilde{h}_{11}[l_1,k_1]=\frac{y_1[l_1,k_1]}{x_1[l_1,k_1]}=h_{11}[l_1,k_1]+\frac{n_1[l_1,k_1]}{x_1[l_1,k_1]}$$
$$\tilde{h}_{21}[l_1,k_1]=\frac{y_2[l_1,k_1]}{x_1[l_1,k_1]}=h_{21}[l_1,k_1]+\frac{n_2[l_1,k_1]}{x_1[l_1,k_1]}. \quad (5)$$

where $[l_1, k_1]$ indicates the location of the scattered pilots colored in red in Fig. 3 (right, top). $\tilde{h}_{11}$ and $\tilde{h}_{21}$ are obtained for the 3 dB boosted scattered pilot cell as the LS estimations of h_{11} and h_{21}, respectively. The CFRs from transmitting antenna #2 (h_{12} and h_{22}) are estimated in the same manner on the 3 dB boosted scattered pilots transmitted by antenna #2 as:

$$\tilde{h}_{12}[l_2,k_2]=\frac{y_1[l_2,k_2]}{x_2[l_2,k_2]}=h_{12}[l_2,k_2]+\frac{n_1[l_2,k_2]}{x_2[l_2,k_2]}$$
$$\tilde{h}_{22}[l_2,k_2]=\frac{y_2[l_2,k_2]}{x_2[l_2,k_2]}=h_{22}[l_2,k_2]+\frac{n_2[l_2,k_2]}{x_2[l_2,k_2]}. \quad (6)$$

here, $[l_2, k_2]$ indicates the location of the scattered pilots colored in red in Fig. 3 (right, bottom). $\tilde{h}_{12}$ and $\tilde{h}_{22}$ are obtained for the 3 dB boosted scattered pilot cell as the LS estimations of h_{12} and h_{22}, respectively. Note that the locations of the CFRs estimated for transmitting antenna #1 in (5) are different from that for transmitting antenna #2 in (6).

In order to obtain the estimated CFR matrix, i.e. $\hat{h}_{11}, \hat{h}_{12}, \hat{h}_{21}$ and $\hat{h}_{22}$, time and frequency interpolation are performed separately on the values of (5) and (6). As the result of the nulling for the scattered pilot, the Doppler limit of channel estimation in time equivalently falls to half compared to SISO. On the other hand, 3 dB higher SNR is obtained in the channel estimation results compared to SISO as the result of the 3 dB boosting.

C. Pilot Boosting

The pilot boosting defines the boosted power level of the scattered pilot compared with the data carriers. The pilot boosting affects the performance, because higher pilot boosting improves channel estimation accuracy. Meanwhile the higher pilot boosting also decreases the power of the data carriers, thus the choice of the pilot boosting is not straightforward. The pilot boosting values for each MIMO SP pattern in ATSC 3.0, which is completely the same as SISO, are listed in Table V. The corresponding power reduction of the data carriers for each SP pattern and pilot boosting is listed in Table VI. The continual and edge pilots are considered to be data carriers to calculate the power reduction values in table VI.

TABLE V
ATSC 3.0 MIMO SCATTERED PILOT BOOSTING POWER

SP Pattern	Boosting Power *b* [dB]				
	0	**1**	**2**	**3**	**4**
MP3_2	0	0	1.40	2.20	2.90
MP3_4	0	1.40	2.90	3.80	4.40
MP4_2	0	0.60	2.10	3.00	3.60
MP4_4	0	2.10	3.60	4.40	5.10
MP6_2	0	1.60	3.10	4.00	4.60
MP6_4	0	3.00	4.50	5.40	6.00
MP8_2	0	2.20	3.80	4.60	5.30
MP8_4	0	3.60	5.10	6.00	6.60
MP12_2	0	3.20	4.70	5.60	6.20
MP12_4	0	4.50	6.00	6.90	7.50
MP16_2	0	3.80	5.30	6.20	6.80
MP16_4	0	5.20	6.70	7.60	8.20
MP24_2	0	4.70	6.20	7.10	7.70
MP24_4	0	6.10	7.60	8.50	9.10
MP32_2	0	5.40	6.90	7.70	8.40
MP32_4	0	6.70	8.20	9.10	9.70

TABLE VI
ATSC 3.0 DATA CARRIER POWER REDUCTION

SP Pattern	Power Reduction [dB]				
	0	**1**	**2**	**3**	**4**
MP3_2	0	0	0.27	0.45	0.64
MP3_4	0	0.14	0.33	0.48	0.59
MP4_2	0	0.08	0.33	0.51	0.65
MP4_4	0	0.17	0.34	0.45	0.57
MP6_2	0	0.16	0.36	0.52	0.63
MP6_4	0	0.18	0.32	0.42	0.51
MP8_2	0	0.18	0.36	0.48	0.60
MP8_4	0	0.17	0.29	0.39	0.46
MP12_2	0	0.19	0.34	0.45	0.54
MP12_4	0	0.16	0.26	0.34	0.40
MP16_2	0	0.19	0.31	0.41	0.49
MP16_4	0	0.15	0.24	0.31	0.36
MP24_2	0	0.17	0.28	0.36	0.42
MP24_4	0	0.14	0.21	0.27	0.31
MP32_2	0	0.16	0.26	0.32	0.38
MP32_4	0	0.12	0.19	0.24	0.27

IV. MIMO PILOT BOOSTING ANALYSIS

In the ATSC 3.0 standardization process, the equalized data signal-to-noise ratio (SNR_{EQ}) was the metric used for obtaining the best overall performance taking into account the pilot boosting value and the channel interpolation method for SISO [7]. SNR_{EQ} was used to design the pilot boosting values for SISO in the standardization process. SNR_{EQ} is estimated as:

$$SNR_{EQ}=\frac{\sigma_S^2\times a}{\sigma_N^2+\sigma_N^2\times f_{\text{int}}/b}=SNR\times\frac{a}{1+f_{\text{int}}/b} \quad (7)$$

where σ_S^2 is the data signal power, σ_N^2 the noise power, b the scattered pilot boosting power compared with the data signal

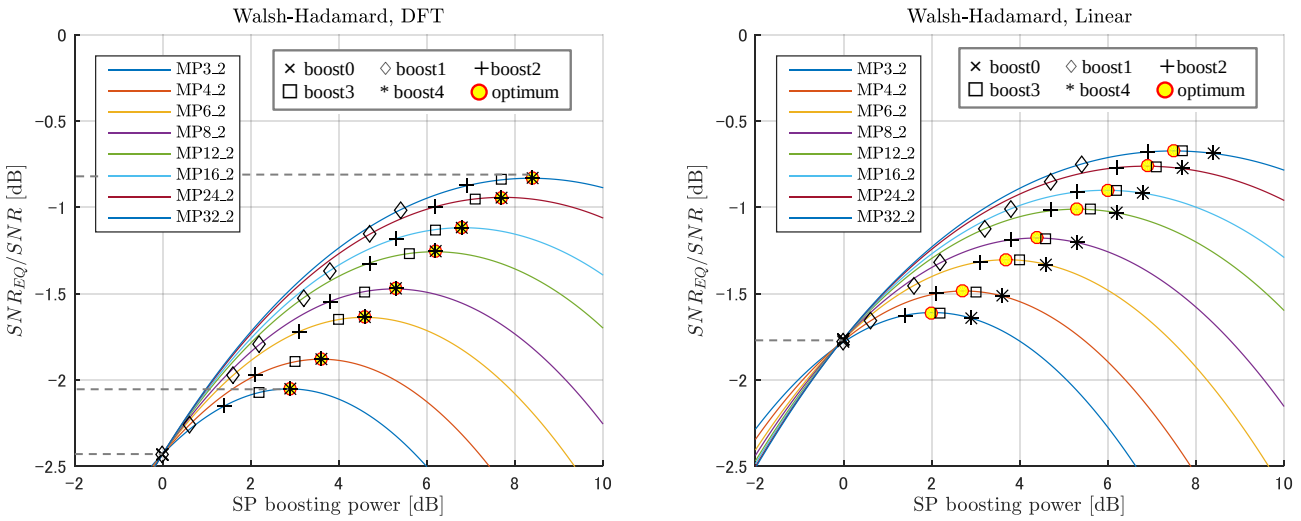

Fig. 4. Equalized SNR performance for D_Y=2 with WH encoding and DFT interpolation (left). With WH encoding and linear interpolation (right).

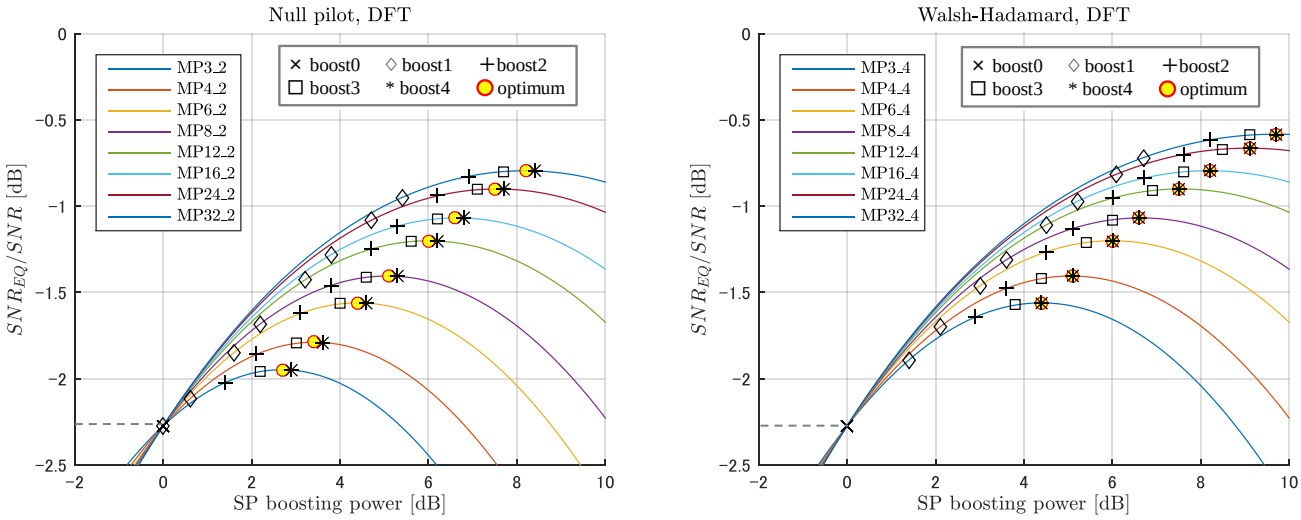

Fig. 5. Equalized SNR performance for D_Y=2 with NP encoding and DFT interpolation (left). D_Y=4 with WH encoding and DFT interpolation (right).

power in linear unit, a the power normalization $a = (D_X \times D_Y)/(D_X \times D_Y - 1 + b)$, and $f_{int} = f_{int,time} \times f_{int,freq}$ is the noise reduction factor by time and frequency interpolation. The value of $f_{int,time}$ was set to {0.750, 0.668} for SISO with D_Y = {2, 4}, which can be calculated from the distance between the two symbols to be linear interpolated [11]. The values of $f_{int,freq}$ varies depending on the receiver design, and the five different boosting values of ATSC 3.0 (from 0 to 4) are standardized for $f_{int,freq}$ = {0, 0.25, 0.5, 0.75, 1}. It should be noted that the pilot boosting value for MIMO is directly adopted the same value as SISO.

The equalized data signal-to-noise ratio for 2x2 MIMO (SNR_{EQ_MIMO}) is considered as:

$$SNR_{EQ\_MIMO} = \frac{\sigma_S^2 \times a}{\sigma_N^2 + 2 \times \sigma_N^2 \times e \times f_{int} / b} = SNR \times \frac{a}{1 + 2 \times e \times f_{int} / b} \quad (8)$$

where e is the noise reduction factor of pilot encoding/decoding process. Note that the noise power caused by the channel estimation error is doubled compared with SISO (7), because the result of MIMO detection is affected by the channel estimation errors from transmitting Antenna #1 and #2. With WH encoding the value of e is set to 0.5, because the channel estimation error is reduced to half by the averaging process following the adding/subtracting the sum and difference of the CFR in (4). With NP encoding, although the value of e is 1, the scattered pilot power b is doubled compared with SISO because of 3 dB boosting. Consequently, SNR_{EQ_MIMO} is equivalent to SNR_{EQ} with the both pilot encoding algorithms in ATSC 3.0.

The value of f_{int} for MIMO pilot can be different from SISO. The value of $f_{int,time}$ remains to {0.750, 0.668} for D_Y = {2, 4} with WH encoding, but {0.668, 0.672} for D_Y = {2, 4} with NP encoding because the equivalent D_Y is doubled. The values of $f_{int,freq}$ and the consequent f_{int} for WH and NP encodings are summarized in Table VII. Whereas the larger D_X offers the smaller $f_{int,freq}$ with linear interpolation, it remains constant with DFT interpolation as it takes into account the Nyquist bandwidth in the interpolation process.

Fig. 4 presents the SNR_{EQ} divided by SNR for D_Y=2 with WH encoding and DFT interpolation (left), and linear interpolation (right) under the noise reduction factors in Table VII. The

TABLE VII
NOISE REDUCTION FACTOR

MIMO Pilot Pattern	Walsh-Hadamard				Null Pilot			
	$f_{int,freq}$		f_{int}		$f_{int,freq}$		f_{int}	
	linear	DFT	linear	DFT	linear	DFT	linear	DFT
MP3_2	0.676	1	0.507	0.750	0.704	1	0.484	0.688
MP3_4	0.676	1	0.465	0.688	0.704	1	0.473	0.672
MP4_2	0.672	1	0.504	0.750	0.688	1	0.473	0.688
MP4_4	0.672	1	0.462	0.688	0.688	1	0.462	0.672
MP6_2	0.669	1	0.502	0.750	0.676	1	0.465	0.688
MP6_4	0.669	1	0.460	0.688	0.676	1	0.454	0.672
MP8_2	0.668	1	0.501	0.750	0.672	1	0.462	0.688
MP8_4	0.668	1	0.459	0.688	0.672	1	0.451	0.672
MP12_2	0.667	1	0.500	0.750	0.669	1	0.460	0.688
MP12_4	0.667	1	0.459	0.688	0.669	1	0.449	0.672
MP16_2	0.667	1	0.500	0.750	0.668	1	0.459	0.688
MP16_4	0.667	1	0.459	0.688	0.668	1	0.449	0.672
MP24_2	0.667	1	0.500	0.750	0.667	1	0.459	0.688
MP24_4	0.667	1	0.458	0.688	0.667	1	0.448	0.672
MP32_2	0.667	1	0.500	0.750	0.667	1	0.459	0.688
MP32_4	0.667	1	0.458	0.688	0.667	1	0.448	0.672

higher SNR_{EQ}/SNR corresponds to the lower degradation due to the channel estimation. The selectable five different boosting (left), boost4 corresponds exactly to the optimum boosting, because $f_{int,freq}$ = 1 with DFT interpolation and the boosting value of boost4 is designed to be optimum for the receiver with $f_{int,freq}$ = 1. With the higher D_X, the higher optimum amplitude is obtained. Note that the gain in SNR_{EQ}/SNR obtained by the optimum pilot boosting from boost0 is at most 0.4 dB in MP3_2, and over 1.5 dB with MP32_2 in Fig. 4 (left).

Fig. 4 (right) presents SNR_{EQ}/SNR with frequency linear interpolation. The optimum boosting becomes smaller than that of DFT interpolation depicted in Fig. 4 (left), because $f_{int,freq}$ of linear interpolation is smaller than DFT interpolation. Fig. 4 (right) indicates that boost2 or boost3 are optimum in this configuration and that the optimization on SP boosting power yields less gain compared with DFT interpolation. It is considered that the smaller $f_{int,freq}$ reduces the noise power in the channel estimation result, hence the smaller boosting is enough to obtain the best performance. SNR_{EQ}/SNR for boost0 is better by 0.7 dB with linear interpolation than DFT interpolation, i.e. SNR_{EQ}/SNR = -2.45 dB for DFT interpolation and -1.75 dB for linear interpolation in Fig. 4 (left) and Fig. 4 (right), respectively.

Fig. 5 (left) shows SNR_{EQ}/SNR for D_Y=2 with NP encoding and DFT interpolation. The optimum boosting for NP becomes slightly smaller than that of WH encoding in Fig. 4 (left), because the noise reduction factor $f_{int,time}$ is smaller than WH encoding. The value of boost4 was standardized to be optimum for SISO only with $f_{int,time}$ = {0.750, 0.668} for D_Y = {2, 4}. Hence for NP encoding boost4 does not correspond perfectly to the optimum boosting value. Fig. 5(left) shows that boost3 or boost4 are optimum in this configuration. Note that SNR_{EQ}/SNR for boost0 is better by 0.2 dB with NP encoding than WH encoding, i.e. SNR_{EQ}/SNR = -2.45 dB for WH and -2.25 dB for NP. This gain is considered to be introduced by the 3 dB boosting in SP power.

Fig. 5 (right) presents SNR_{EQ}/SNR for D_Y =4 with WH encoding and DFT interpolation. Boost4 corresponds to the optimum boosting. The gain obtained by the optimization on pilot boosting power with D_Y = 4 becomes greater than D_Y = 2. SNR_{EQ}/SNR for boost0 is better by 0.2 dB with D_Y = 4 than D_Y = 2, i.e. SNR_{EQ}/SNR = -2.25 dB for D_Y = 4 and -2.45 dB for D_Y = 2 in Fig. 5 (right) and Fig. 4 (left), respectively. This gain is introduced by the noise reduction factor $f_{int,time}$.

V. METHODOLOGY AND SIMULATION SETUP

The performance of MIMO scattered pilot is evaluated by physical layer simulations. The transmitter chain complies with the ATSC 3.0 specification. MIMO channel estimation algorithms described in Section III have been implemented.

The two MIMO pilot encoding schemes are compared in terms of Bit Error Rate (BER) after BCH. Moreover the Mean Squared Error (MSE) between the estimated channel and the real channel is also evaluated. MSE is defined as:

$$MSE = E_{l,k}\left[\frac{1}{4}\sum_{j=1}^{2}\sum_{i=1}^{2}\left\|h_{ij}[l,k]-\hat{h}_{ij}[l,k]\right\|^2\right] \quad (9)$$

where $h_{ij}[l, k]$ and $\hat{h}_{ij}[l,k]$ denote the real and estimated CFR of receiving antenna #*i* and transmitting antenna #*j* for carrier *k* of the OFDM symbol number *l*, respectively. $E[\cdot]$ refers to the expectation calculation.

Both mobile and fixed reception scenarios have been considered with the NGH mobile outdoor channel [12] and a simple two path SFN channel, respectively. The NGH mobile outdoor channel is a fast fading model composed of eight taps shown in Table VIII. The SFN channel models a fixed receiver located between two MIMO transmitters using two configuration parameters: the power imbalance (PI) which gives the difference between the received signal levels from the two transmitters and the delay time between the received signals. In the following section, the PI = 3 dB, the delay time τ = 0.5 GI duration and the frequency offset = 0 Hz are used for a typical fixed reception for SFN environment.

The basic transmission parameters for simulations are shown in Table IX. In the simulation parameters, FFT size, modulation and GI ratio are selected to be the same as the operational parameters in current DTT system ISDB-T in Japan [13]. The required SNR of the current service for SISO rooftop reception is about 20 dB [14]. Using 64NUC 12/15, the SNR for MIMO would be about the same threshold with the same total transmitting power as SISO (i.e. half power in each antenna). The mobile reception service known as One-Seg, which targets

TABLE VIII
TAP VALUES OF NGH MOBILE OUTDOOR CHANNEL

Tap number	Excess delay [μs]	h_{11}, h_{22} [dB]	h_{12}, h_{21} [dB]
1	0	-4.0	-10.0
2	0.1094	-7.5	-13.5
3	0.2188	-9.5	-15.5
4	0.6094	-11.0	-17.0
5	1.109	-15.0	-21.0
6	2.109	-26.0	-32.0
7	4.109	-30.0	-36.0
8	8.109	-30.0	-36.0

TABLE IX
BASIC PARAMETERS FOR EVALUATION

FFT size	8k
Number of carriers	6913
Signal bandwidth	5.83 MHz
Modulation and code rate	QPSK 5/15 64 NUC 12/15
GI pattern	GI5_1024 (GI ratio: 1/8, GI length: 148 μs)
MIMO scattered pilot encoding	Walsh-Hadamard Null Pilot
Frequency Interpolation	DFT Linear

at handheld terminals and launched on April 1st 2006 in Japan, has been provided with QPSK 2/3 with SISO [15], and the QPSK 5/15 is selected as the parameters to provide the same capacity with MIMO. It is assumed that the cross polarization discrimination (XPD) is infinite as an ideal case (AWGN), 18 dB as a practical fixed reception scenario (SFN) and 6 dB for the mobile reception scenario (Rice, NGH outdoor) [12], [16]. The performance is evaluated with a minimum mean-square error equalizer [17]. Long LDPC codes (64k) and non-uniform constellations standardized in ATSC 3.0 are used [18]. Convolutional Time Interleaver (CTI) with the parameter N_{rows}=724 (time interleaving depth of approximately 100 ms) is adopted and frequency interleaving is also applied. The SNR is defined as the ratio of the total signal power (antenna #1 and #2) to the noise power at each receiver (either antenna #1 or #2) in the following part. The required SNR is defined as the SNR to achieve BER = 10^{-4} in this paper.

VI. SIMULATION RESULTS

A. *Pilot Boosting*

We evaluated the optimum pilot boosting with the densest pilot pattern MP3_2 with the parameters in Table IX. The BER performance comparison for SP boosting with WH encoding and DFT interpolation is shown in Fig. 6. Here, XPD is set to be infinite and AWGN channel is used to evaluate the ideal condition. The result showed that the best performance is achieved with pilot boost4 or boost3, and the gain is 0.3 dB at BER = 10^{-4}. It is assumed that the gain can be larger for a stricter BER criterion. Therefore, the analysis of the equalized SNR (Fig. 4, left) has a consistency with the BER evaluation results.

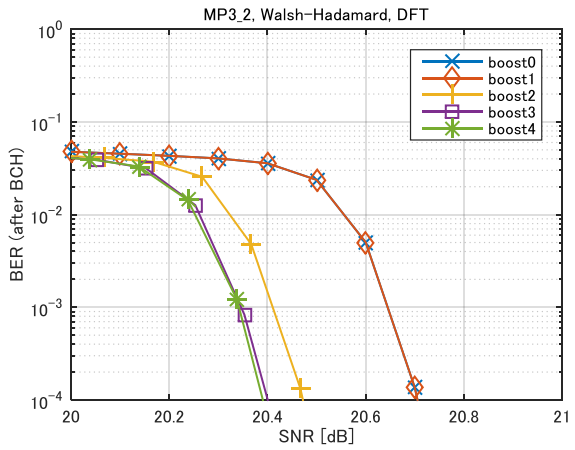

Fig. 6. BER comparison for pilot boosting with MP3_2, Walsh-Hadamard encoding and DFT interpolation in AWGN channel.

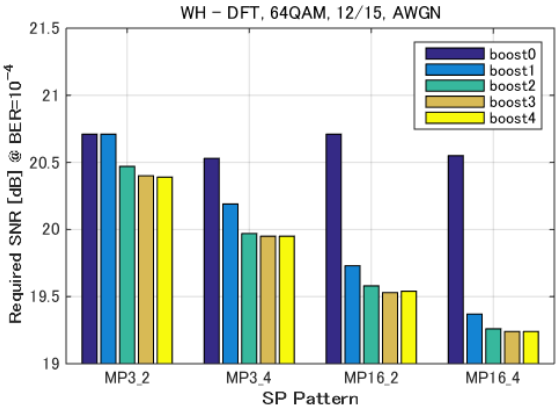

Fig. 7. Required SNR comparison for MIMO pilot pattern with Walsh-Hadamard encoding and DFT interpolation in AWGN channel.

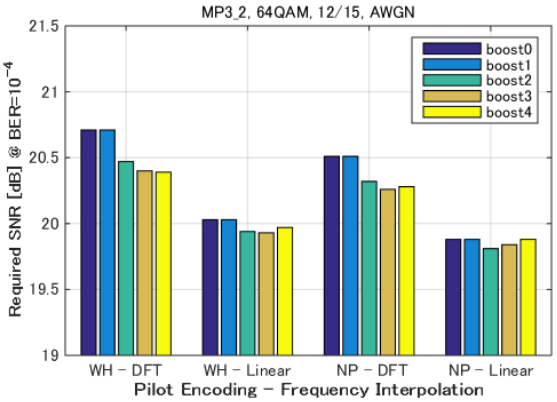

Fig. 8. Required SNR comparison for MIMO pilot encoding and frequency interpolation with MP3_2 in AWGN channel.

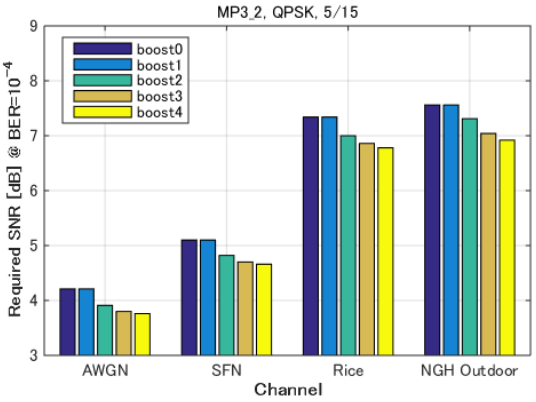

Fig. 9. Required SNR comparison for different channel realization with MP3_2, Walsh-Hadamard and DFT interpolation.

Fig. 7 shows the required SNR for several SP patterns with WH encoding and DFT interpolation. The transmission parameters in Table IX are used. The result showed that the best performance is achieved with pilot 4 or boost3 for all SP patterns. The gain of MP3_4 from MP3_2 with boost0 is 0.2 dB and the gain becomes the same value theoretically calculated from Fig. 4(left) and Fig. 5 (right). The gain of boost4 from boost0 becomes over 1 dB with MP16_2 and MP16_4. These

results conclude that the boosting value should be selected carefully with higher D_X and D_Y, but the best boosting is boost4 or boost3 regardless of pilot pattern.

Fig. 8 shows the required SNR comparison for several SP configurations with MP3_2. The transmission parameters in Table IX are used. Compared with DFT interpolation, linear interpolation shows better performance by about 0.7 dB for WH encoding with boost0 as described in Fig. 4 (left) and Fig. 4 (right). It can be also observed that NP-DFT shows 0.2 dB better result than WH-DFT with boost0 as mentioned in Fig. 4 (left) and Fig. 5 (left), because of the smaller $f_{\text{int,freq}}$. We confirmed that the best boosting value varies depending on the configuration, e.g. the best boosting is boost4 or boost3 for DFT interpolation but boost3 or boost2 for linear interpolation.

Fig. 9 shows the required SNR comparison for AWGN, SFN, Rice (K factor = 10) and NGH outdoor (maximum Doppler frequency: F_d =33.3 Hz) with MP3_2 and WH-DFT. The transmission parameters in Table IX are used with QPSK 5/15. This result indicates that the best boosting value is boost4 for all channels, which keeps a consistency with the equalized SNR analysis shown in Fig. 4. Additionally, the gain introduced by the pilot boosting is constant regardless of the channel. It is confirmed that the gain obtained by the pilot boosting optimization with QPSK 5/15 in AWGN is almost the same as 64NUC 12/15 (WH-DFT in Fig. 8). From these result, the optimum boosting value is considered as an independent parameter from the modulation and code rate.

The simulation results concluded that boost3 is practically the best pilot boosting for all configurations evaluated in this paper. In the following section, we conducted the performance evaluation with boost3.

B. Frequency Interpolation

We compared two common interpolation algorithms, i.e. DFT and linear interpolation, for the frequency interpolation with both MIMO pilot encoding schemes. Fig. 10 shows MSE comparison with both MIMO pilot encoding schemes in the SFN channel. The other parameters are the same described in Table IX. This result showed that MSE of linear interpolation converges on a value that is the estimation error caused by the frequency interpolation.

Fig. 11 shows MSE comparison in the SFN channel with SNR = 20 dB and different delays. This result showed that the error increases gradually as the delay time increases. In this result, linear interpolation achieved slightly lower MSE than DFT interpolation because of the smaller $f_{\text{int,freq}}$ with short delay echoes. However, linear interpolation is gradually degraded as the delay time increases because of the frequency interpolation error. It is confirmed that MSE of WH-Linear is rapidly increased with long echoes due to the virtually double D_X. DFT interpolation showed lower MSE than linear interpolation with long delay echoes up to GI (148 μs) regardless of the MIMO pilot encoding. Comparing WH and NP, NP showed slightly better MSE because of the 3dB pilot boosting and the smaller $f_{\text{int,time}}$.

The BER performance in the SFN channel is shown in Fig. 12. This result shows a consistency with MSE evaluation in Fig. 10, i.e. NP-DFT shows the best performance in BER and also the lowest MSE at around SNR = 23 dB. In addition, it is confirmed that Quasi Error Free (QEF) is not achieved with WH-Linear configuration in the SFN channel, because the MSE is higher than the required SNR.

Fig. 13 shows MSE comparison for different MIMO pilot encoding with MP3_2 in NGH outdoor channel (F_d = 33.3 Hz). This result shows that MSE of all configurations converges on a value around -25 dB that is the tracking error for the time varying channel. Note that the MSEs in Fig. 13 become straight lines in the low SNR region (below 10 dB), because the SNR is

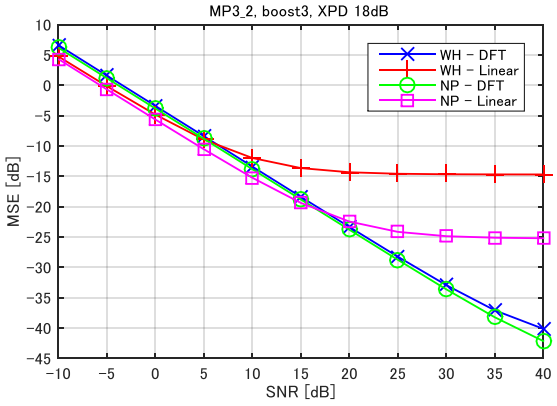

Fig. 10. MSE comparison with MP3_2 in SFN channel (PI = 3dB, τ =0.5 GI).

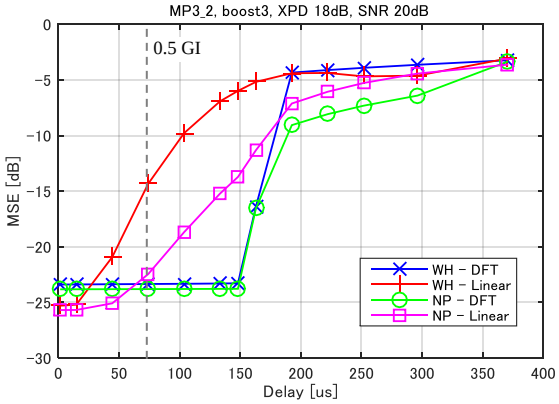

Fig. 11. MSE comparison with MP3_2 in SFN channel (PI = 3dB, SNR = 20 dB).

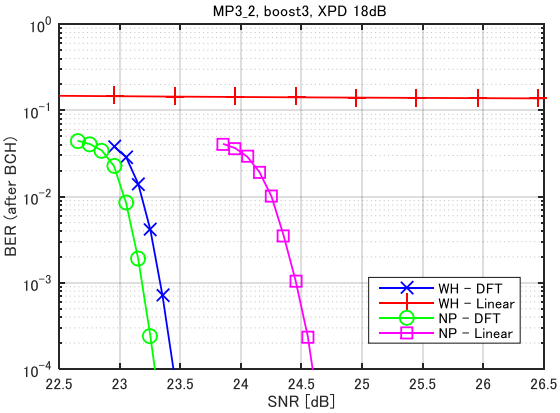

Fig. 12. BER comparison with MP3_2 in SFN channel (PI = 3dB, τ =0.5 GI) with 64NUC 12/15.

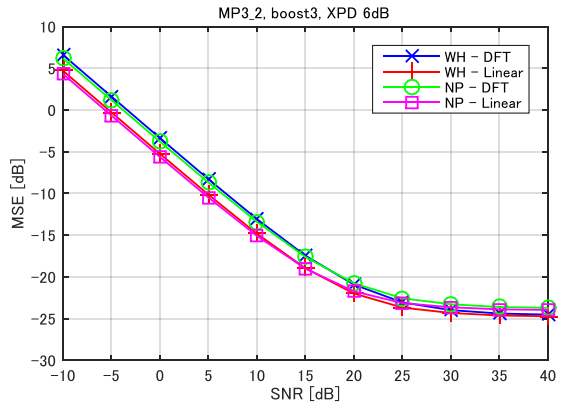

Fig. 13. MSE comparison with MP3_2 in NGH Outdoor channel (F_d = 33.3Hz).

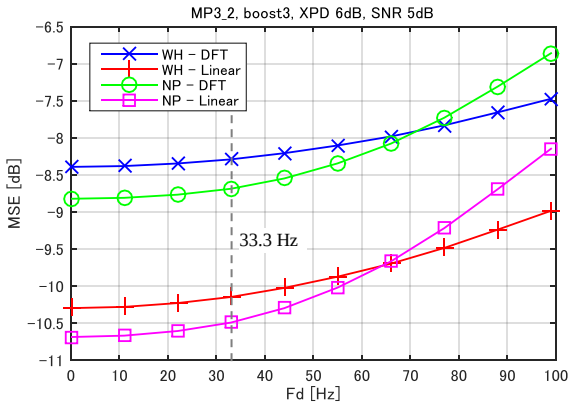

Fig. 14. MSE comparison with MP3_2 in NGH Outdoor channel (SNR = 5 dB).

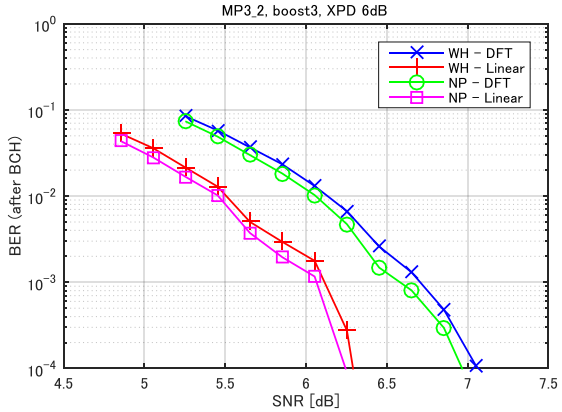

Fig. 15. BER comparison with MP3_2 in NGH Outdoor channel (F_d = 33.3Hz) with QPSK 5/15.

dominant compared with the tracking error.

Fig. 14 shows MSE comparison in the NGH outdoor channel with SNR = 5 dB for different maximum Doppler frequency. This result shows that the error increases gradually as the maximum Doppler frequency increases. In low F_d region, NP showed slightly better MSE than WP because of the 3dB pilot boosting and the smaller $f_{\text{int,time}}$. However, MSE of NP is rapidly increased in high Doppler frequency channel because the tracking error is increased due to the virtually doubled D_Y. In this result, linear interpolation showed better performance than DFT interpolation for all F_d spans with both MIMO pilot encoding schemes. It is considered that the noise reduction factor for the channel estimation is dominant in such a low SNR region.

The BER performance with QPSK 5/15 in NGH outdoor channel is shown in Fig. 15. It is confirmed that NP-Linear is the best performance in BER. This result shows a consistency with MSE evaluation, i.e. the lowest MSE is obtained with NP-Linear at around SNR = 6 dB in Fig. 13. It is considered that the channel is composed of some short echoes (up to 8.1 μs delay in time), thus linear frequency interpolation works well.

The simulation results concluded that DFT interpolation is better for the SFN channel to cope with long echoes. On the other hand, linear interpolation works well in a mobile channel in which only short delay echoes exist. Especially, since the tracking error is much smaller than the SNR, linear interpolation is better than DFT because of the smaller noise reduction factor. It should be noted that the DFT interpolator is defined as $f_{\text{int,freq}}$ = 1 in this paper. The conclusion that linear interpolation is better in a mobile channel can vary if the DFT interpolator is implemented with the smaller $f_{\text{int,freq}}$.

C. *MIMO Scattered Pilot Recommendation*

We evaluated the optimum MIMO scattered pilot configuration for fixed/mobile reception scenario with several GI/FFT combinations. The GI length is a parameter selected by broadcasters depending on the required coverage, i.e. network configuration, geographical condition and the required distance between the SFN transmitters. First, we evaluated the required SNR in three SFN scenarios, i.e. with short GI (GI1_192: 28 μs), middle GI (GI5_1024: 148 μs) and long GI (GI7_2048: 296 μs) for all the FFT size. The simulation parameters are summarized in Table X.

Fig. 16 shows the required SNR for GI5_1024 with all the allowed SP configurations for each FFT size. The results of WH and NP encoding are shown in solid and dashed line, respectively. The results are grouped according to D_X, e.g. 8k-D_X3-WH presents the results for MP3_2 and MP3_4 with 8k FFT and WH encoding. The values of SP overhead, 16.7 % and 8.3 %, correspond to MP3_2 and MP3_4 in 8k-D_X3-WH. The result shows that NP encoding provides slightly better performance than WH with the same SP overhead. It is considered that 3 dB pilot boosting and the smaller $f_{\text{int,time}}$ introduces this gain. From the point of FFT size, larger FFT achieves the same Nyquist limit with the sparser SP patterns and better performance with the smaller $f_{\text{int,freq}}$.

Fig. 17 and Fig. 18 describe the results with GI1_192 and

TABLE X
PARAMETERS FOR MIMO PILOT RECOMMENDATION

FFT size	8k	16k	32k
Number of carriers	6913	13285	27649
Signal bandwidth	5.83 MHz		
Modulation and code rate	64 NUC 12/15 for SFN channel QPSK 5/15 for NGH Outdoor		
MIMO scattered pilot encoding	Null Pilot Whalsh-Hadamard		
Frequency Interpolation	DFT for SFN channel Linear for NGH Outdoor		
Pilot boosting	boost3		

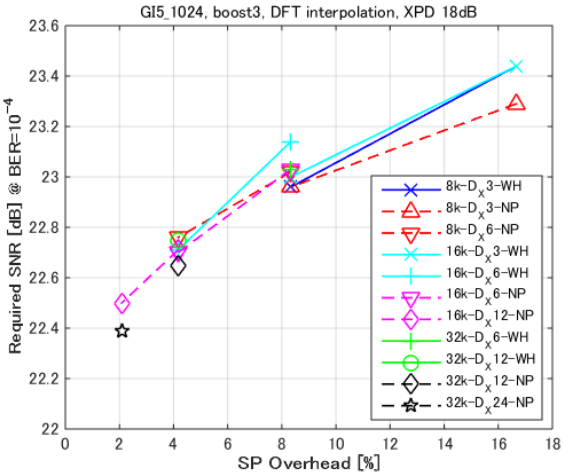

Fig. 16. Required SNR comparison in SFN channel (PI = 3dB, τ =0.5 GI) with GI5_1024 and 64NUC 12/15.

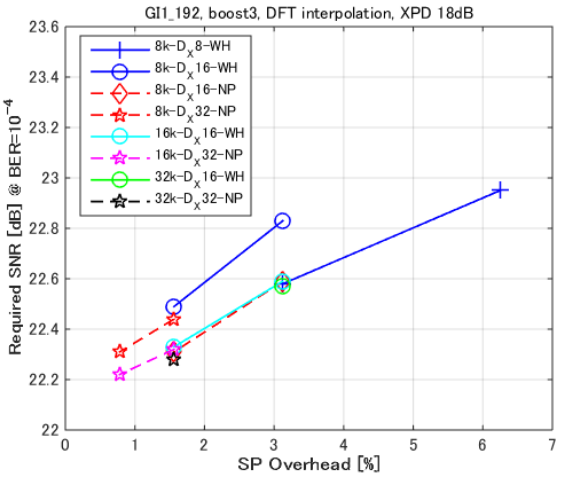

Fig. 17. Required SNR comparison in SFN channel (PI = 3dB, τ =0.5 GI) with GI1_192 and 64NUC 12/15.

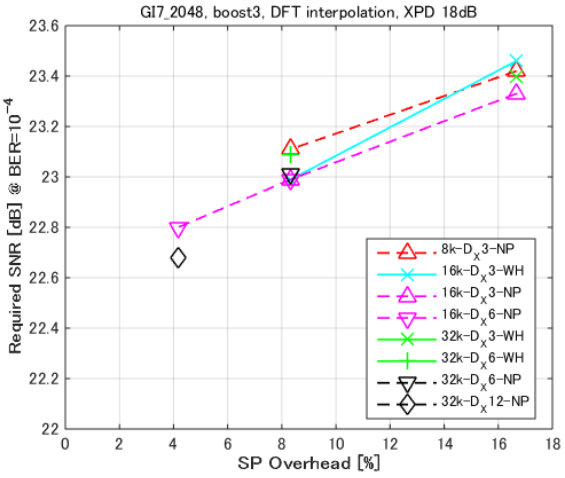

Fig. 18. Required SNR comparison in SFN channel (PI = 3dB, τ =0.5GI) with GI7_2048 and 64NUC 12/15.

GI7_2048. NP encoding showed better performance than WH regardless of GI duration. With short GI case, the required SNR becomes the lowest with the sparsest SP because of the smallest $f_{\text{int,freq}}$. We conclude that NP encoding with larger FFT size and

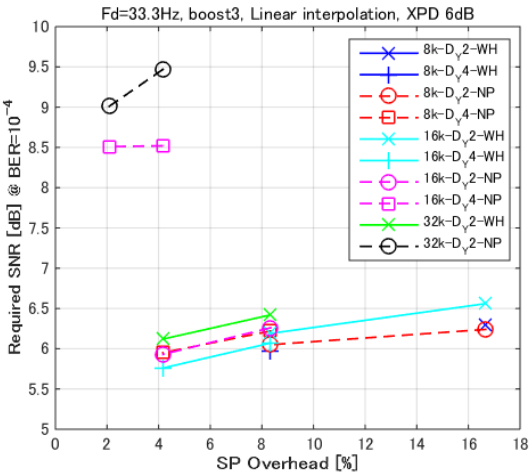

Fig. 19. Required SNR comparison in NGH Outdoor channel (F_d = 33.3 Hz) with GI5_1024 and QPSK 5/15.

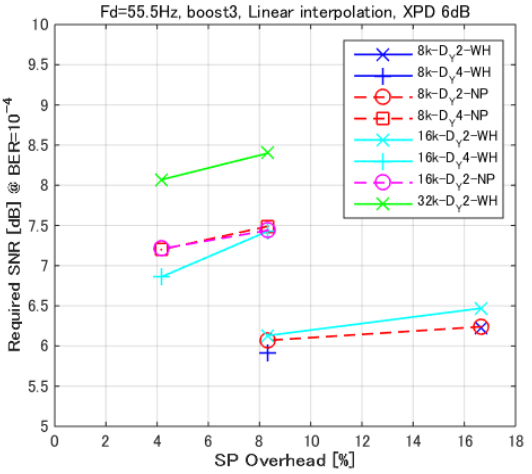

Fig. 20. Required SNR comparison in NGH Outdoor channel (F_d = 55.5 Hz) with GI5_1024 and QPSK 5/15.

larger D_X SP pattern is the best configuration for fixed reception scenario, such as the time invariant SFN channel.

Next, we evaluated the required SNR in two NGH outdoor scenarios with a middle speed and a high-speed reception. GI5_1024 and the simulation parameters in Table X are used.

Fig. 19 shows the result in a middle speed reception (F_d = 33.3 Hz, 60 km/h@600 MHz) with all the allowed SP configurations for GI5_1024. The result showed that the performance of NP encoding with 16k-D_Y4 and 32k-D_Y2 are degraded to a large extent compared with the other configurations. It is considered that the equivalent D_Y is doubled in NP encoding scheme, thus the performance in the time varying channel is severely degraded especially with larger FFT and larger D_Y.

Fig. 20 shows the result in a high-speed reception (F_d = 55.5 Hz, 100 km/h@600 MHz) with GI5_1024. The worst configurations, 16k-D_Y4-NP and 32k-D_Y2-NP, are excluded here. The simulation indicated that WH shows slightly better performance than NP with the same SP overhead. Comparing 16k-D_Y4-WH and 32k-D_Y2-WH, it is confirmed that the performance with 32k FFT is degraded in such a high-speed

time varying channel even with $D_Y = 2$. We conclude that WH encoding with smaller FFT size and smaller D_Y is the best configuration for mobile reception scenario.

VII. Conclusion

This paper evaluates the two MIMO pilot encoding algorithms adopted in ATSC 3.0, known as Walsh-Hadamard and Null Pilot encoding. Regarding the pilot boosting evaluation, a theoretical analysis and a physical layer simulation considering two channel interpolation algorithms, namely DFT interpolation and linear interpolation for frequency interpolation, conclude that boost3 is a practical option as the optimum pilot boosting for both pilot encoding algorithms. The pilot boosting values were standardized for SISO, but the five different boosting values cover the optimum boosting values for MIMO. It is confirmed that the optimum pilot boosting greatly improves the performance especially with higher D_X and D_Y and that the maximum gain in required SNR becomes over 1.5 dB.

Based on the optimization of the pilot boosting described above, the optimum MIMO pilot configuration including pilot pattern and pilot encoding algorithm for fixed/mobile reception scenario is evaluated by physical layer simulations. The studies were conducted with different channels, a SFN channel for fixed reception and DVB-NGH outdoor channel for mobile reception. From the simulation results in a fixed SFN channel, it can be observed that Null Pilot encoding provides better performance than Walsh-Hadamard encoding and that larger D_X SP pattern is the best configuration. The simulation results confirmed that larger FFT size can reduce the pilot overhead and achieve lower required SNR in a fixed-time invariant SFN channel. In long echo SFN channel, DFT interpolation provides better performance than linear interpolation in terms of the frequency interpolation at the receiver. In contrast, it was confirmed that Walsh-Hadamard encoding with smaller D_Y SP pattern is the best configuration in a high Doppler time varying mobile channel. From the simulation results in DVB-NGH outdoor channel, it can be observed that smaller FFT size and linear interpolation at the receiver can achieve the lowest required SNR. It should be noted that Null Pilot encoding is rapidly degraded especially with (16k FFT, D_Y=4) or (32k FFT D_Y=2) in time varying channel because of the virtually doubled D_Y and that Walsh-Hadamard encoding with linear frequency interpolation can be severely degraded in frequency selective fading channel because of the virtually doubled D_X.

References

[1] L. Fay, L. Michael, D. Gomez-Barquero, N. Ammar, and M. W. Caldwell, "An overview of the ATSC 3.0 physical layer specification," *IEEE Trans. Broadcast*., vol. 62, no. 1, pp. 159-171, Mar. 2016.

[2] D. Gomez-Barquero, C. Douillard, P. Moss and V. Mignone, "DVB-NGH: The Next Generation of Digital Broadcast Services to Handheld Devices," *IEEE Trans. Broadcast*., vol. 60, no. 2, pp. 246-257, June 2014.

[3] D. Gomez-Barquero *et al*, "MIMO for ATSC 3.0," *IEEE Trans. Broadcast*., vol. 62, no.1, pp. 298-305, Mar. 2016.

[4] S. Saito *et al*, "8K Terrestrial Transmission Field Tests Using Dual-Polarized MIMO and Higher-Order Modulation OFDM," *IEEE Trans. Broadcast*., vol. 62, no.1, pp. 306-315, Mar. 2016.

[5] I. Eizmendi, *et al*, "DVB-T2: The Second Generation of Terrestrial Digital Video Broadcasting System," *IEEE Trans. Broadcast.*, vol. 60, no. 2, pp. 258-271, June 2014.

[6] K. Manolakis, *et al*, "Performance Evaluation of a 3GPP LTE Terminal Receiver," *Proc. 14th European Wireless Conference 2008*, Prague, Czech Republic.

[7] E. Garro, J. Joan Gimenez, S.-I. Park, and D. Gomez-Barquero, "Scattered Pilot Performance and Optimization for ATSC 3.0," *IEEE Trans. Broadcast*., vol. 63, no. 1, pp. 282-291, Mar. 2017.

[8] M. K. Ozdemir and H. Arslan, "Channel estimation for wireless OFDM systems," *IEEE Commun. Surveys Tuts.*, vol. 9, no. 2, pp. 18–48, 2nd Quart., 2007.

[9] M. J. Fernandez-Getino Garcia, J. M. Paez-Borrallo and S. Zazo, "DFT-based channel estimation in 2D Pilot Symbol Aided OFDM Wireless Systems," *Proc. IEEE VTC Spring 2001*, vol. 2, pp. 810-814.

[10] A. Dowler, A. Doufexi, and A. Nix, "Performance evaluation of channel estimation techniques for a mobile fourth generation wide area OFDM systems," *Proc. IEEE VTC Fall 2002*, Vancouver, Canada.

[11] ETSI 102 831, "Digital Video Broadcasting (DVB); Implementation guidelines for a second generation digital terrestrial television broadcasting system (DVB-T2)".

[12] P. Moss, T. Y. Poon, and J. Boyer, "A simple model of the UHF cross-polar terrestrial channel for DVB-NGH," Research & Development White Paper WHP205, Sept. 2011.

[13] ITU-R Recommendation BT.1306-6: "Error-correction, Data Framing, Modulation and Emission Methods for Digital Terrestrial Television Broadcasting," Nov. 2011.

[14] ITU-R Recommendation BT.2036-1: "Characteristics of a reference receiving system for frequency planning of digital terrestrial television systems," July 2016.

[15] ARIB STD-B31 Version 1.6: "Transmission system for digital terrestrial television broadcasting," Nov. 2005.

[16] ITU-R Recommendation BT.419-3: "Directivity and polarization discrimination of antennas in the reception of television broadcasting," June 1990.

[17] P. Fertl *et al*, "Performance Assessment of MIMO-BICM Demodulators Based on Mutual Information," *IEEE Trans. Signal Processing*., vol. 60, no. 3, pp. 1366-1382, Mar. 2012.

[18] L. Michael and D. Gomez-Barquero, "Bit-Interleaved Coded Modulation (BICM) for ATSC 3.0," *IEEE Trans. Broadcast.*, vol. 62, no. 1, pp. 181-188, Mar. 2016.

Takuya Shitomi received the M. Eng. degree in systems science from Tokyo Institute of Technology, Japan, in 2005. He joined Japan Broadcasting Corporation (NHK) in 2005. He is a research engineer in the Advanced Transmission System Research Division in NHK Science and Technology Research Laboratories (STRL) in Tokyo. He is currently pursuing the Ph.D. degree in terrestrial broadcasting with the Mobile Communications Group, Institute of Telecommunications and Multimedia Applications (iTEAM), Universitat Politecnica de Valencia (UPV), Spain.

His research activities are focused on terrestrial digital broadcasting system and MIMO transmission technology. He has participated in the standardization process of ATSC 3.0, within the ModCod Ad-Hoc Group.

Eduardo Garro received the M.Sc. Degree in telecommunications engineering and the second M.Sc. degree in communications and development of mobile services from Universitat Politecnica de Valencia (UPV), Spain, in 2013 and 2014, respectively. He is currently pursuing the Ph.D. degree in terrestrial broadcasting, where he is a Researcher and Developer with the Mobile Communications Group, Institute of Telecommunications and Multimedia Applications (iTEAM). During his doctoral studies, he has been a Guest Researcher with Electronics and Telecommunications Research Institute, South Korea.

In 2012, he joined the iTEAM, working with Agencia Nacional del Espectro, the spectrum regulator of Colombia on the coexistence between DTT and 4G (LTE) technologies. He has also participated on the planning and optimization of DVB-T2 networks in Colombia.

His research activities are focused on layered division multiplexing systems and realistic channel estimations for broadcasting networks. He is a current member of the ATSC forum and has been actively participating during the ATSC 3.0 standardization process.

Kenichi Murayama received his M. Eng. degree in mechanical engineering from Niigata University, Japan in 1996. He joined Japan Broadcasting Corporation (NHK) in 2002. From 2002 to 2008, he worked in the NHK Engineering Administration Department and Transmission & Audience Reception Engineering Center. From 2008, he is a research engineer in the Advanced Transmission Systems Research Division in NHK Science and Technology Research Laboratories (STRL) and engaged in research and development related to the next generation of digital terrestrial broadcasting. He has participated in the standardization process of ATSC 3.0.

David Gomez-Barquero received the M.Sc. degree in telecommunications engineering from the Universitat Politecnica de Valencia (UPV), Spain, and the University of Gävle, Sweden, in 2004, and the Ph.D. degree in telecommunications from the UPV in 2009. He was Post-Doctoral Researcher with the Fraunhofer Heinrich Hertz Institute, Germany.

He is a Senior Researcher (Ramon and Cajal Fellow) with the Institute of Telecommunications and Multimedia Applications, UPV, where he leads a research group working on next generation wireless broadcasting technologies. He held visiting research appointments with Ericsson Eurolab, Germany, the Royal Institute of Technology, Sweden, the University of Turku, Finland, the Technical University of Braunschweig, Germany, the Sergio Arboleda University of Bogota, Colombia, the New Jersey Institute of Technology, USA, and the Electronics and Telecommunications Research Institute, South Korea.

Dr. Gomez-Barquero has been actively participating in the digital television standardization, including DVB-T2, T2-Lite, DVB-NGH and ATSC 3.0. Currently, he is the project manager of the 5G-PPP project 5G-Xcast (Broadcast & Multicast Communication Enablers for the Fifth-Generation of Wireless Systems). He is an Associate Editor of the IEEE Transactions on Broadcasting and the ETRI journal, and he edited the book Next Generation Mobile Broadcasting (CRC Press, 2013).